# Chapter 3
# MIIC: Monitoring and Imaging Based on Interferometric Concepts

**Christoph Sens-Schönfelder, Hortencia Flores-Estrella, Martina Gassenmeier, Michael Korn, Florian Köllner, Claus Milkereit, Ernst Niederleithinger, Stefano Parolai, Marco Pilz, Eraldo Pomponi, Andreas Schuck, Katja Thiemann and Jürgen Völkel**

**Abstract** The capability of seismic interferometry to create virtual sources at receiver sites from records of ambient seismic noise is used for seismic monitoring and tomography of different targets. We present hardware developed specifically for the needs of seismic data acquisition in the context of monitoring and ambient noise tomography. Digitizers are capable of continuous recording and real time wireless data transmission in self organizing meshes to allow for robust telemetry in difficult circumstances such as cities or landslides that may cause the loss of stations. A software tool is described that implements required processing and analysis procedures for the interferometric processing. We have applied the novel 3D ambient noise surface wave tomography approach to the Issyk-Ata fault in Kyrgyzstan. It shows that seismic interferometry can successfully be used for structural investigations on length scales of only 100 m. The method uses 3D sensitivity kernels for a single-step inversion of phase velocity dispersion curves for subsurface S-wave velocity structure and incorporates topography. We recover lateral differences in sediment velocities and an offset of the bedrock depth across the fault. Applications of interferometric monitoring to the geological $CO_2$ storage test site in Ketzin (Germany) and to the Piton de la Fournaise volcano (La Reunion island) emphasize the value

C. Sens-Schönfelder (✉) · M. Gassenmeier · C. Milkereit · S. Parolai · M. Pilz
Helmholtz Centre Potsdam, GFZ German Research Centre for Geosciences, Telegrafenberg, 14473 Potsdam, Germany
e-mail: sens-schoenfelder@gfz-postdam.de

H. Flores-Estrella · M. Korn · E. Pomponi
Leipzig University, Institute for Geophysics and Geology, Talstrasse 35, 04103 Leipzig, Germany

F. Köllner · A. Schuck
GGL Geophysics and Geotechnics Leipzig GmbH, Bautzner Str. 67, 04347 Leipzig, Germany

E. Niederleithinger
BAM Federal Institute for Materials Research and Testing, Unter den Eichen 87, 12205 Berlin, Germany

K. Thiemann · J. Völkel
K-UTEC AG Salt Technonogies, Am Petersenschacht 7, 99706 Sondershausen, Germany

M. Weber and U. Münch (eds.), *Tomography of the Earth's Crust: From Geophysical Sounding to Real-Time Monitoring*, Advanced Technologies in Earth Sciences,
DOI: 10.1007/978-3-319-04205-3_3, 

of this approach. At Ketzin site we identify variations of the subsurface velocities that are correlated with changes in the ground water level and mask potential signals from the reservoir depth. At Piton de la Fournaise volcano, seismic velocity changes are linked to volcanic processes as shown by comparison with surface displacement and seismicity that are typically used to characterize volcanic activity. We observe a clear distinction between phases of inflation prior to eruptions and deflation during periods of quiescence.

## 3.1 Introduction

For the realization of interferometric time series analyses, the utilization of coherent phase information in complex wave fields is essential. In the context of elastic waves and, in particular, for the extraction of phase velocities from ambient noise, the first seismological application making use of this idea was presented by Aki (1957). He proposed to deduce information about the subsurface from the spatial correlation of the noise field, which is assumed to be random due to distributed and uncorrelated sources continuously exciting elastic waves. In contrast to this spatial correlation, Poupinet et al. (1984) demonstrated that the complex scattered wave field recorded after an excitation of elastic waves in a heterogeneous medium such as the earth's crust shows temporal correlation as well. The noise's correlation properties are controlled by the propagation medium regardless of the wave field's complexity, and if the medium is stationary, the waveforms will be, too. This allows to monitor changes in the subsurface by comparing waveforms recorded at different times.

These investigations established the basic concepts of what is now referred to as seismic interferometry (Curtis et al. 2006). However, to boost the development of applications using the spatial and temporal coherence of complex wave fields like noise and seismic coda, it took another essential finding: Only the experimental observation—and later also the mathematical confirmation—that the impulse response or Green's function of the elastic medium can be retrieved directly from diffuse wave fields increased the interest in such signals and accelerated research.

Focusing on the use of seismic interferometry for the investigation of the subsurface, the MIIC project (Monitoring and Imaging based on Interferometric Concepts) as part of the GEOTECHNOLOGIEN program contributes to this development. Special attention is given to the transfer and application on different length scales ranging from centimeters in laboratory over geotechnical scales to even kilometers in seismological applications. According to the project's structure, this article is organized in three parts, whereof the first describes technical developments of hard- and software. In the second part, we concentrate on imaging applications employing seismic interferometry to obtain high-resolution structural information about the subsurface. The third and last part is devoted to monitoring, where the permanent presence of seismic noise is used to continuously follow the evolution of the target medium.

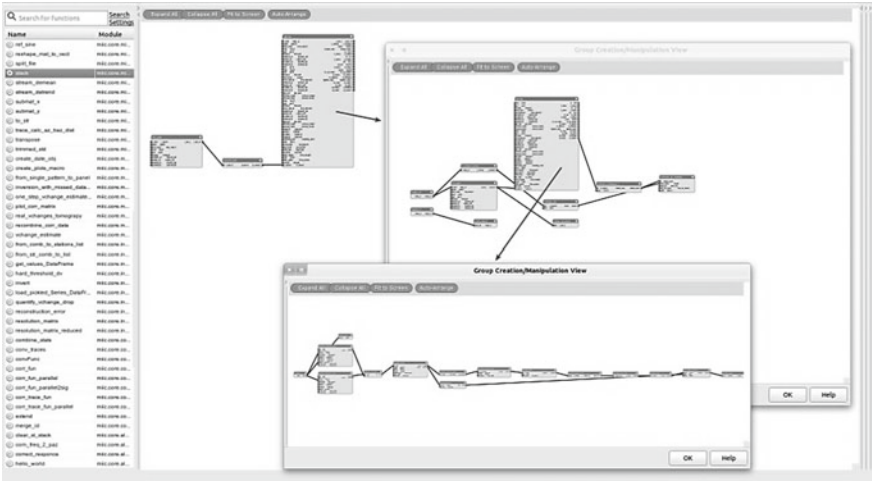


**Fig. 3.1** Graphical user interface of MIIC library showing the data flow through the processing functions. To structure the processing, different tasks are grouped in blocks that are edited in a hierarchy

## 3.2 Technical Developments

The concepts of seismic interferometry profoundly changed the use of seismic data and introduced new lines of data analysis. To facilitate the application of the new approaches we developed within MIIC project a Python based program library for typical analysis procedures, and instruments for the continuous recording of ground motion in distributed networks with real time data transmission.

### *3.2.1 The MIIC Software Suite for Interferometric Processing of Seismic Data*

Many of the steps involved in interferometric processing are technically simple but not within the initial scope of established seismological analysis software. The MIIC software suite now provides this functionality. It is available via svn from http://theo1.geo.uni-leipzig.de/svn. The core of the MIIC software is a Python library organized in different modules for various processing tasks. A graphical user interface facilitates the creation of processing routines by visualizing connections and dependencies of variables and by checking the consistency of data types.

The graphical user interface is based on a visual environment called blockcanvas (https://github.com/enthought/blockcanvas) in which functions are represented by blocks and data by wires. In Fig. 3.1 a screenshot of a processing flow with nested blocks is shown.

The library behind this interface uses the core functions of the ObsPy toolbox (Megies et al. (2011), https://github.com/obspy) for data import and handling of raw seismological data. It contains functions for the typical routines of data pre-processing such as sign-bit normalization or spectral whitening. Cross-correlation which usually is the most CPU-time consuming part of the processing is implemented as a multi-process routine that optionally uses multiple cores of the system. A new data structure is defined for cross-correlations, which holds meta-information of the two participating stations, about the original data as well as information that are specific to the correlation.

Assessing temporal variations requires a further data structure: a set of correlations from a single station pair generated from the noise that was recorded at different times—a correlation matrix. A specific module is dedicated to the processing of this data structure. It implements filtering, trimming, normalization, smoothing and functions to estimate temporal variations of the correlation functions such as apparent stretching due to changes in the subsurface velocity and shifting of the correlation functions as a consequence of clock drifts.

Results can be visualized directly or exported into image files. To facilitate the interface with other software for further analysis or visualization the data structures can be saved into MatLab® files. The documentation is available at http://theo1.geo.uni-leipzig.de/docs.

### *3.2.2 Seismic Sensors for Continuous Recording with Wireless Real Time Access*

To meet the specific requirements of the application of interferometric concepts for data acquisition optimized instruments, being low-cost and allowing for near real-time data transmission and continuous recording, have been developed in the project. The instruments are based on the SOSEWIN system, originally developed by the Helmholtz-Zentrum Potsdam - Deutsches GeoForschungsZentrum (GFZ) and Humboldt University of Berlin (see Fleming et al. 2009 and Fig. 3.2).

This system employs advances in various technologies to incorporate off-the-shelf sensors with processing and communications components into low-cost seismic sensing units that are linked by advanced, robust and rapid communications routing and network organizational protocols appropriate for wireless mesh networks. The reduced cost of the instruments (less than one tenth of a standard instrument) allows creating dense, self-organizing and decentralized seismic imaging and monitoring networks of up to hundreds of nodes. In particular, its self-organizing capability, allows the system to adapt continuously to changing circumstances, i.e., the addition/removal/malfunctioning of nodes and interference in communications due to local (and possibly time-varying) phenomena. This is particularly important for monitoring purposes since some of the sections of the network might be lost following landslides, earthquakes, etc.

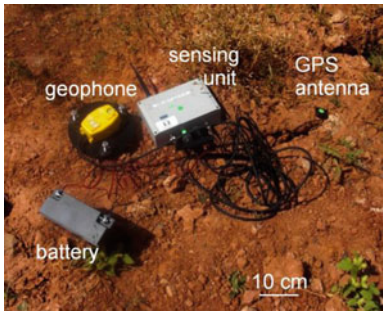


**Fig. 3.2** Field use of the wireless sensing unit (top right) connected with one 4.5 Hz Geophone. During 2D array seismic noise measurements, which generally involve period of recording of few hours, the necessary energy can be provided by small 17 Ah batteries (*bottom left*)

Moreover, each sensing unit also has the capacity to measure other environmental parameters (temperature, humidity, etc.). This allows to obtain also detailed images of environmental impacts. At the same time, the stations also create a wireless mesh network by which the data required for efficient interferometric monitoring and imaging can be transmitted via WiFi to a computer that belongs to the network. This is different from standard seismological equipment and allows a preliminary analysis of the data directly in the field.

Therefore, the system can provide real-time information for use in seismic 3D imaging and 4D monitoring of changes in the subsoil conditions, environmental parameters as well as soil-structure interactions. Due to their lower cost the much higher instrumental density means that analysis tools can rely more on real data and less on interpolation schemes. This is particularly important since the system functionality can be extended also to early warning (e.g. activation of landslides after earthquakes).

## 3.3 Shear-Wave Velocity Imaging of Complex Shallow Structures

The shear wave velocity $v_s$ is a key parameter related to the assessment of the local amplification of ground motion and is most commonly used in engineering seismology. Within this context, shear wave velocity values can be measured in situ by means of various invasive (borehole) or non-invasive (shear wave refraction and reflection studies) techniques. Although these techniques provide accurate and well resolved values of $v_s$ they suffer from several drawbacks, such as increasing costs with required depth or only pointwise estimates.

In recent years, passive seismic techniques have received considerable attention and have become increasingly attractive in a broad range of seismological disciplines on different scales (e.g. Bonnefoy-Claudet et al. 2006). This kind of techniques are generally low cost and carried out with instruments that are easy to deploy, and are not bound to any active sources. The success of these applications is explained by the fact that passive methods are based on surface waves, which are by far the strongest waves excited in the seismic noise wave field.

Among the passive methods seismic interferometry has particularly become popular in a variety of applications in the recent years (see reviews by Campillo 2006; Curtis et al. 2006 among many others). One of the most intriguing applications of the method, shown both theoretically and experimentally, is that a random wavefield has correlations, which, on average, take the form of the Green's function of the media (e.g. Rickett and Claerbout 1999; Lobkis and Weaver 2001; Weaver and Lobkis 2001; Snieder 2004). Between pairs of receivers, the Green's function can be extracted from cross-correlations of ambient noise recorded at both receivers, allowing an estimate of the propagation delay between the stations. So far, such travel time measurements of Rayleigh waves reconstructed from seismic noise have mainly been used at lower frequencies to produce high-resolution images on continental and regional scales whereas only very few studies exist so far showing the applicability of the method for higher frequencies on the local scale (Chávez-García and Luzón 2005; Brenguier et al. 2007; Picozzi et al. 2009).

Here we introduce a new method for a one-step tomographic inversion scheme for obtaining 3D shear-wave velocity models. The method, which also works in complex environments with significant topography, is based on the micro-array recordings of seismic noise (i.e. the deployment of a number of 10–20 stations distributed over the area of interest) for a few hours. Thereon, Rayleigh wave phase velocities have to be determined for each interstation ray path, e.g. based on the frequency domain SPAC technique of Aki (1957). Therefore we make use of the possibility to substitute an average over time of the correlation in the frequency domain between two stations for a fixed interstation distance instead of the azimuthal average of the correlation required by SPAC (Weaver and Lobkis 2004). The basic idea of this hypothesis is that the average of the cross-correlation between two stations for a long enough time window averages all the different directions of the waves composing the microtremors, i.e., a single station pair can be seen as being equivalent for an azimuthal average of many station pairs with the same interstation distance. In this context, Curtis and Halliday (2010) clearly highlight the importance of a suitable distribution of noise sources in all directions around the station pair of interest.

In order to confirm this, for a one line profile we have used seismic noise records excited by a non-synchronized source, such as a person jumping, near the first receiver of the profile. With the cross-correlation of these records (using the first receiver as reference) we obtain seismic sections that are comparable to those from standard active source data, showing the reliability of high frequency seismic noise interferometry.

With these seismic sections we calculate frequency ($\omega$)—slowness ($p$) transforms following Forbriger (2003). In Fig. 3.3 we show the ($\omega$, $p$)-spectrum obtained for the seismic section obtained from the cross-correlations of the non-synchronized noise and for the active source seismic section. The most prominent signals in these figures correspond to the fundamental mode of Rayleigh waves. Additionally, both spectra show high slowness values (around 5 s km$^{-1}$) for low frequencies (10 Hz) which might be due to a shallow water table that can cause a different depth for the shallow velocity changes for P and S-waves. For the two kinds of sources the emergence of

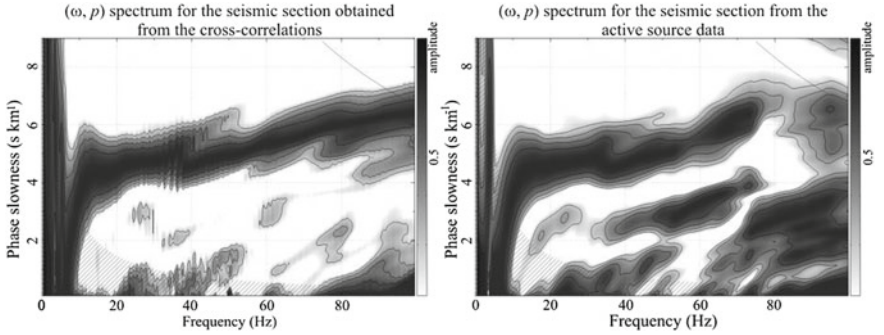


**Fig. 3.3** ($\omega$, $p$) spectra for a line profile (34, 5 m long) for two sets of data. *Left* for the seismic section obtained from the cross-correlations of the non-synchronized noise. *Right* for the seismic section of the active source data. Both sources were located next to the first receiver. The *grey scale* indicates the modulus of the complex wave field obtained by the transform

potential osculation points that indicate the presence of different modes with similar slowness is visible at around 30 Hz.

The main difference between these spectra is the emergence of the first higher mode of surface waves in the transformation of the active source data (35–75 Hz and 2.5–3.7 s km$^{-1}$), which is not visible in the spectrum of the interferometric signal. This might be due to the fact that with the cross-correlation of records with multiple modes spurious events are generated losing information about higher modes (Halliday and Curtis 2008).

From these results we can confirm that even if the majority of sources are clustered in a narrow azimuthal range (a person jumping near the first receiver of a line profile) the travel time information is stable, providing enough energy coming from the remaining azimuthal sectors (Derode et al. 2003).

Using seismic noise recorded by an instrumental array we can determine the travel times for all ray paths between the sensors. The first step of data processing consists of preparing the waveform data from each individual station. Since our interest lies in detecting local variations in $v_s$ for the shallowest part of the subsurface and since the distances of the array only span a range of some meters to around one hundred meters, we are strongly interested in high frequency noise (higher than a few Hz) where Rayleigh waves are prevalent.

Therefore, a suitable high-pass filter should be applied to the data aiming to improve the signal-to-noise ratio for the high-frequency range of interest, and to oppress the influence of large-amplitude low-frequency signals that tend to obscure noise signals. After preparing the time series, one-bit normalized data were used to calculate the cross-correlations for all interstation pairs, following Campillo and Paul (2003) and Bensen et al. (2007). The calculated cross-correlations are stacked for all selected frequencies and for each pair of receivers to improve the signal-to-noise ratio (Bensen et al. 2007). Finally, the travel times between all stations are calculated from the estimated phase velocities using the known distances between sensors.

Although the ray path is velocity dependent, meaning that travel time inversion is a non-linear problem, deviations of the paths from a straight line will be sufficiently small. Therefore, a bias of a few percent can be tolerated to keep the solution linear, and the medium of interest can be subdivided into a reasonable number of smaller cells so that the problem can be expressed in a simple discrete matrix form.

Starting from a homogeneous 3D velocity model for the entire medium of interest, an iterative procedure using singular value decomposition, for minimizing the misfit between the observed and theoretical travel times, can be adopted (Picozzi et al. 2009; Pilz et al. 2012, 2013). In particular, the measured slowness along each ray path contains information about the underlying structure to depths corresponding to approximately one-third to one-half the wavelength of each frequency (Foti et al. 2009).

To account for the fact that shallow blocks are sampled more intensely than deeper ones, we introduce a further constraint on the solution which weights the data depending on the number, length, orientation, and vertical penetration depth of each ray path segment crossing each cell. When running the inversion procedure the weights for all cells, and accordingly the velocity vectors, are updated after each iteration step until a reasonable compromise between the reduction of the rms error between the observations and the predictions and the norm of the solution is reached. Finally, the updated slowness $s$ is used to calculate the 3D shear wave velocity structure using the relation with the Rayleigh wave slowness by $v_s = (0.92s)^{-1}$.

As an example Fig. 3.4 shows the inversion results of the array recordings obtained after 500 iterations across the Issyk-Ata fault in Kyrgyzstan, a moderately dipping thrust to reverse fault defining the northern deformation front for the central Tien Shan between ~74°E and ~75°E longitude. A clear difference in S-wave velocity is observed, contrasting the northern and the southern parts of the studied area and running in an east-west direction parallel to the fault. The transition zone is rather sharp, spanning only some tens of meters. A distinct low-velocity wedge in the uppermost part of the northern section of the studied area can be identified (reddish color in Fig. 3.4) which might be caused by fault scarp weathering and present-day detritus which had slid off from the rock terrace. In this interpretation, formation of the colluvial wedge would represent multiple faulting events with a total displacement of around 10 m.

The estimated absolute $v_s$ values are robust and compatible with the findings of previous studies for similar material in Bishkek (Parolai et al. 2010). Below the low-velocity deposits the material can be interpreted as late Pleistocene and Holocene terraces whereas Pliocene conglomerates with dense carbonate cement with gravel stones form the high velocity bluish part in the south (Korjenkov et al. 2012, Fig. 3.4). Remarkably, this novel approach has identified two parallel fault structures, one lowering the Tertiary by nearly 30 m, and the other lowering the top of the Tertiary strata to greater, but unresolved, depths to the north.

This means that, based on the correlation of seismic noise recordings and using a limited number of seismic stations and recording times of several tens of minutes, detailed images of the local subsoil structure can be obtained even under pronounced topographic conditions. In contrast to information gained from traditional

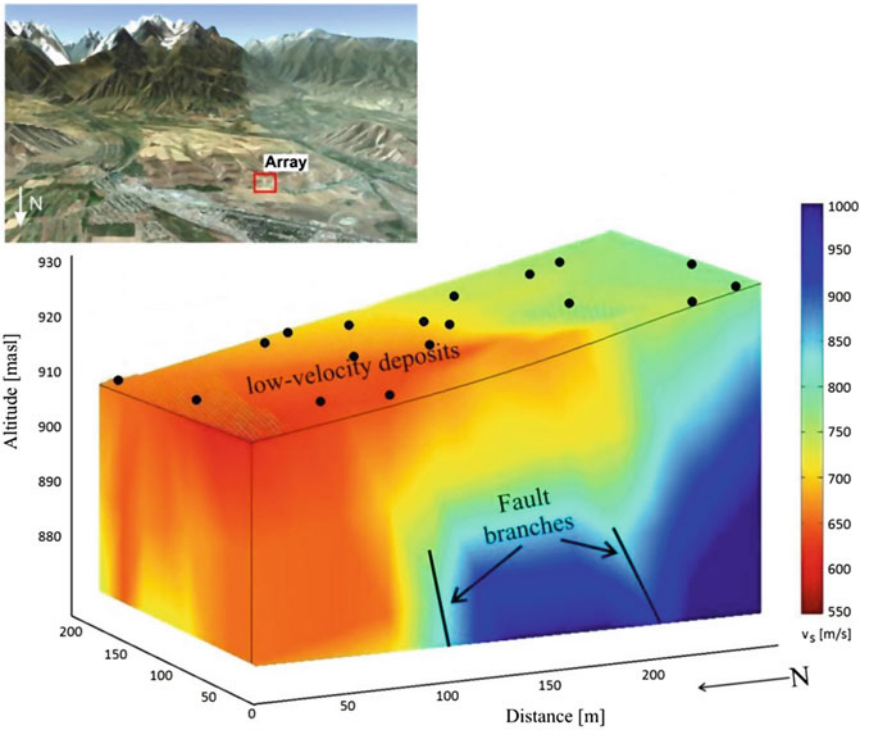


**Fig. 3.4** *Top* Satellite image showing the southern outskirts of Bishkek facing the Ala-Too range. The topography is exaggerated by a factor of two. Location of the array measurement is indicated. Google Earth, © 2012, CNS Spot Image © 2012, Digital Globe © 2012. *Bottom* Inversion results of measurements on the Issyk-Ata fault obtained after 500 iterations. The topography is amplified about 3 times. The *dots* represent locations of the sensors

2D trench excavation, such seismic imaging methods can add an extra dimension and a deeper perspective. The presented technique is particularly advantageous since it can return useful information about the heterogeneous subsurface structure and structural changes therein in complex environments across seismic faults or areas prone to landslides almost in real time even if earthquakes do not occur. Such information about the S-wave velocity distribution is difficult to acquire with traditional methods, simply analyzing the ambient noise field by the means described here can serve as a reliable and economical alternative.

## 3.4 The Monitoring of Seismic Velocity Variations with Ambient Seismic Noise

As shown in the previous section, the concepts of seismic interferometry allow to obtain information about subsurface structure from records of ambient seismic noise. Furthermore, the permanent presence of this signal also allows to investigate dynamic

processes that alter the elastic properties of the subsurface. The above described methodology can be used to monitor temporal variations in the medium with high spatial resolution by repeated imaging if the wave speed variations caused by changes in the mechanical characteristics of the subsurface material exceed a few percent (the uncertainty of the velocity estimates). While this, together with the necessary length of acquired seismic noise signal, is particularly suitable for engineering applications, other approaches can be considered when the velocity changes in geological materials that are caused by natural processes like deformation in volcanoes or co-seismic stress changes in fault zones are of smaller amplitude.

When high temporal resolution at large spatial scale is required or when subtle temporal variations of the order of a fraction of a percent are to be investigated Coda Wave Interferometry, CWI (Poupinet et al. 1984; Snieder et al. 2002; Sens-Schönfelder and Wegler 2006) is a more appropriated approach. However, the higher and excellent accuracy of velocity change estimates below 0.1 % is obtained by using multiply scattered coda waves with unknown propagation paths. This uncertainty causes a degradation of spatial resolution.

Two important properties of this method are of relevance: firstly, coda waves reconstructed from seismic noise are not as sensitive as direct waves to changes of the noise properties e.g. its dominant direction. Secondly the long propagation time of coda waves allows for amplification of small velocity changes to significant time shifts which increases the accuracy but lowers the spatial resolution.

The concept of applying coda wave interferometry to noise correlation functions is discussed in Sens-Schönfelder and Wegler (2011). Here we discuss applications to seismic monitoring at the $CO_2$ storage test site in Ketzin (Germany) and present an approach to image changes of seismic velocities at Piton de la Fournaise Volcano on La Reunion Island (France).

### *3.4.1 Monitoring Subsurface Changes at the $CO_2$ Storage Test Site in Ketzin*

Regarding the potential risk of unwanted migration of carbon dioxide and the expense of active seismic investigations, we test the feasibility of monitoring a $CO_2$-storage-testsite in Ketzin (Brandenburg, Germany) with CWI.

Since June 2008, supercritical $CO_2$ is injected in an anticlinal saline aquifer of about 80 m thickness, the Stuttgart Formation, at a depth of approximately 650 m (Fig. 3.5a). With a nearly constant injection rate, more than 60.000 tons of $CO_2$ have been injected from 2008 until the beginning of 2012, which is a relatively small amount, compared to other offshore injection sites.

3D time-lapse monitoring between 2005 and 2011 (Ivanova et al. 2012) indicates an asymmetric $CO_2$ plume, with an extension of 250 m in N-S direction and about 350 m in the E-W direction, with larger quantities of $CO_2$ in the western part.

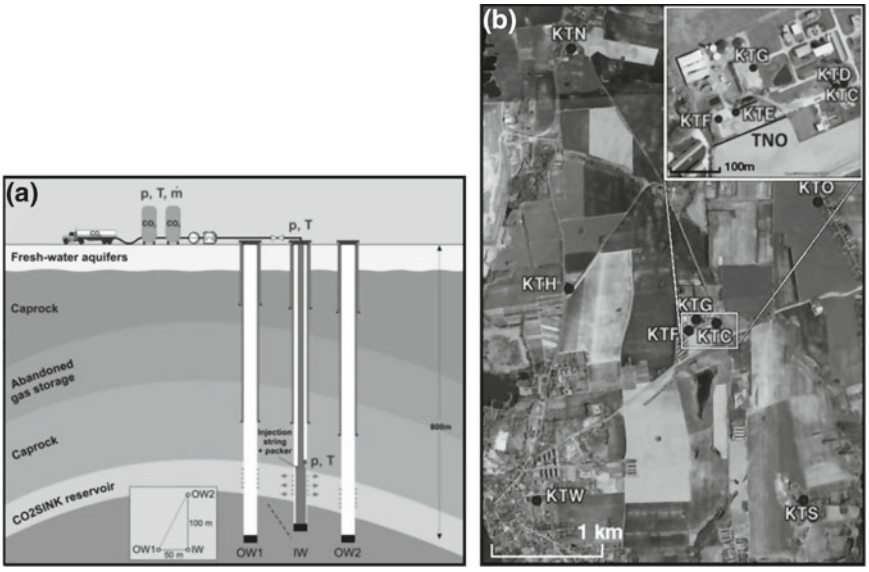


**Fig. 3.5** **a** Scheme of CO2 injection in a saline aquifer at 650 m depth (http://www.co2sink.org/techinfo/injection.htm). **b** Station-map of Ketzin with close-up of the injection site

We operated a seismic network around the test-site from May 2008 (before the start of the injection) until June 2010, consisting of three-component Guralp seismometers with a sampling rate of 100 Hz. During February 2011 the network was re-equipped, extended and operated until February 2012. The number of receivers in the network was increased from 5 (in 2008) up to 10 receivers (in 2011) in distances from tens of meters up to a few kilometers around the injection site (Fig. 3.5b).

To retrieve estimates of the Green's functions between the seismic stations, pairwise cross-correlation of one hour long segments was applied after rotation of the horizontal components into R- (parallel to inter station azimuth) and to T- coordinates (perpendicular to inter station azimuth), followed by the usual preprocessing (trend removal, down sampling, 1 bit normalization). The cross-correlations are asymmetric and dominated by a phase traveling with about 300 m/s, which is consistent with Rayleigh waves propagating in the shallow sediments (Fig. 3.6a).

We analyzed the correlation functions for possible velocity changes using the stretching method of Sens-Schönfelder and Wegler (2006). Due to the fact that the long term average injection rate is almost constant, we expect a monotonic decrease of seismic velocities. We observe velocity variations with all station and component combinations that show a cyclic behavior of approximately one year period, which cannot be caused by the $CO_2$ injection (Fig. 3.7a).

In order to characterize the depth distribution of the velocity changes, we analyzed moving time windows after the direct arrival with a velocity of 300 m/s. The analysis in the frequency range of 1.5–3 Hz showed that the amplitude of the annual velocity

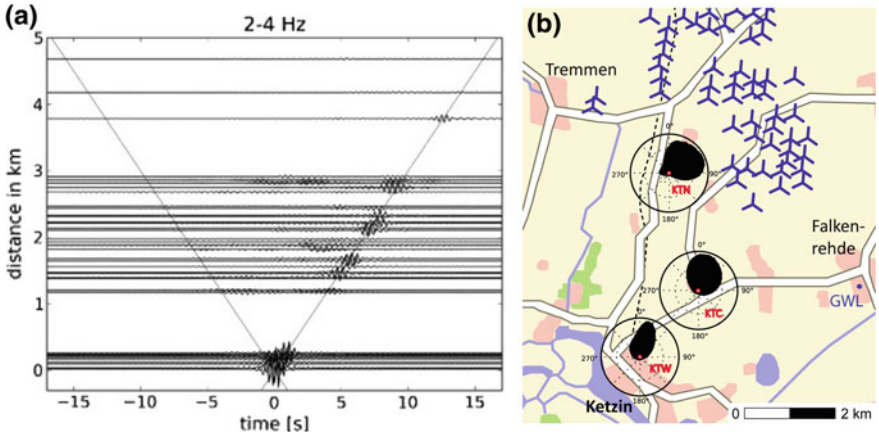


**Fig. 3.6** **a** Time distance section of cross-correlations at 2–4 Hz, a velocity of 300 m/s is indicated with lines. **b** Map of the Ketzin area with histograms of measured noise directions pointing towards a wind park (at 2–2, 4 Hz, http://www.havelland-flaeming.de)

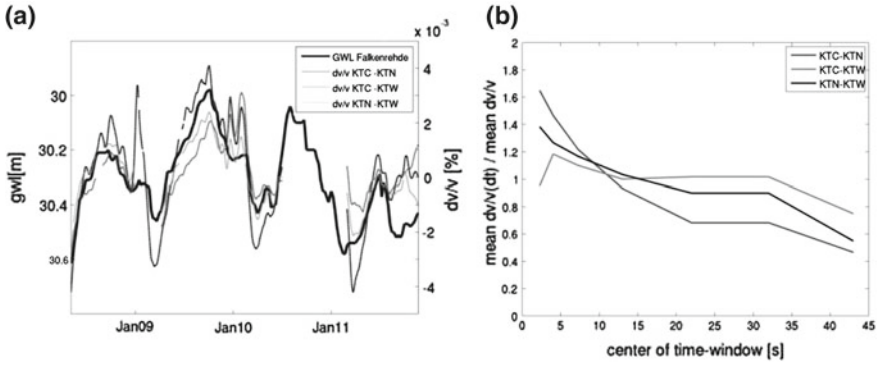


**Fig. 3.7** **a** Ground water level and mean velocity change averaged over all time-windows and components for three station combinations at 1, 5–3 Hz. **b** Lapse time dependence of the velocity changes as the ratio of velocity change at a particular time-window to mean velocity change

variations decreases in time windows in later parts of the coda (Fig. 3.7b). As shown by Obermann et al. (2013) such an observation can be explained with velocity changes that occur in the shallow subsurface. As the changes are periodic and shallow, we suspect a meteorological influence. A comparison of the velocity changes to ground water level (GWL) measurements in a well in Falkenrehde, which is approximately 3, 5 km north-west of the injection site, shows a clear correlation between the phases of the velocity changes and the GWL (Fig. 3.7a).

To exclude the possibility that variations of the noise source locations, that might also show an annual periodicity, cause the apparent velocity variations, we analyzed the prominent direction of the noise. Under the assumption of a dominance of Rayleigh waves on the vertical component, which was confirmed in several tests,

we calculated the backazimuth of the dominant propagation direction by maximizing the coherence between the Hilbert transform of the vertical component and the horizontal component rotated to point in the noise direction. The analysis showed a good stability of the noise direction, and therefor excludes the noise-field itself as a cause for the velocity variations.

The observed directions of the noise measured at KTC, KTN and KTW point in the direction of a wind park, whereby the distribution for KTW, which is furthest away, is more narrow as the distribution for KTC and KTW, which are closer to the wind park and thus show a broader distribution of azimuths of incident wave field (Fig. 3.6b). This distribution is stable throughout the analyzed period.

We can thus confirm that the observed periodic velocity variations are not related to modifications in the noise sources distribution but caused by changes in the GWL. These periodic variations mask potential signals of material changes at the reservoir depths.

### *3.4.2 Velocity Monitoring at Piton de la Fournaise Volcano*

Piton de la Fournaise Volcano on La Reunion Island (France) in the Indian Ocean was one of the first places where the concept of monitoring temporal variations of the seismic velocity with noise correlation functions was applied. It is one of the most active volcanoes on Earth with usually more than one basaltic eruption per year.

During the period from mid-1999 until end of 2000 Brenguier et al. (2008) observed long term variations of the seismic velocities with unknown origin that are interrupted by short term drops before eruptions. Based on this temporal coincidence Brenguier et al. (2008) suggested to use the velocity variations as an indicator for upcoming eruptions. Here we use a densified network to investigate the relation between the spatial distribution of velocity changes and different processes affecting the volcano.

In 2009 the seismometer network at Piton de la Fournaise was densified by the UnderVolc research program (Brenguier et al. 2012). The seismic network is indicated in Fig. 3.9 by green dots together with the GPS network operated by the Observatoire volcanologique du Piton de la Fournaise that we use as one indicator of the volcanic activity.

We calculate noise correlation functions as described above and estimate velocity changes from their coda for all available station pairs. This results in 210 curves of velocity changes that represent the dynamics of the volcano. The variations of the velocity are not homogeneously distributed in space as measurements show a clear systematic depending on the participating stations. To infer the spatial distribution of velocity changes we have to make an assumption about the spatial sensitivity of the measurements. We therefore assume that coda waves propagate in the multiple scattering regime which concentrates the sensitivity around the stations. Under this assumption we invert the velocity changes measured at station pairs for changes at the location of individual stations. Figure 3.8 shows these station-wise velocity changes

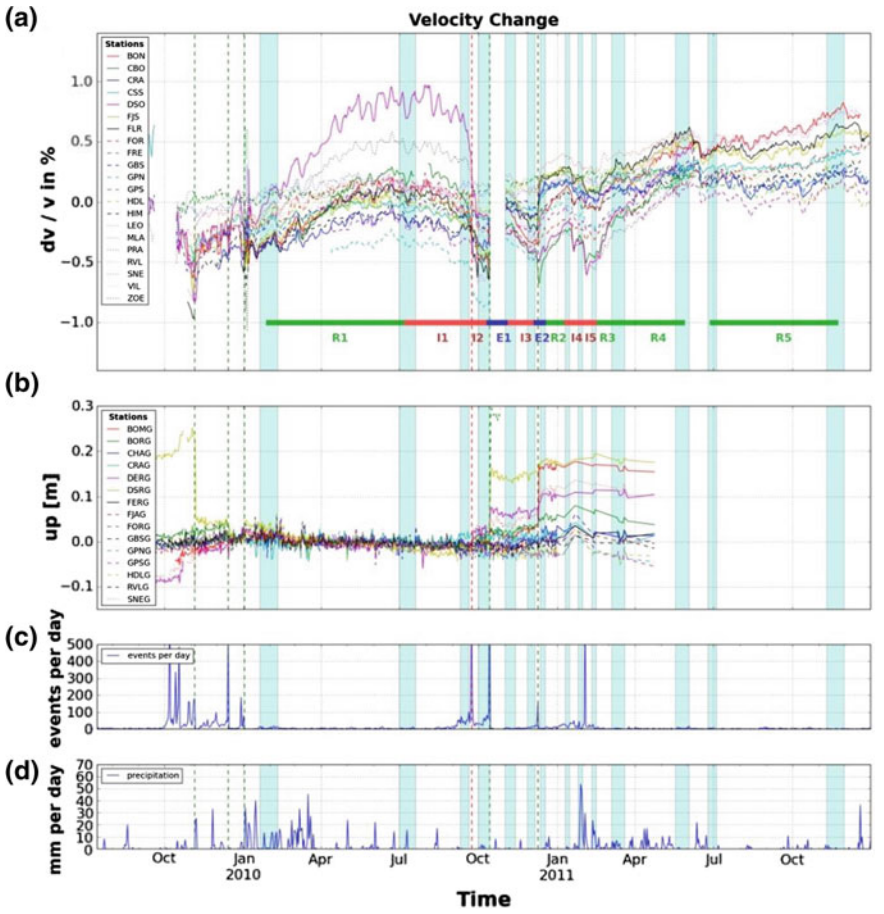


**Fig. 3.8** **a** Velocity changes at the seismic stations. **b** Upward component of the surface deformation. **c** Daily number of seismic events in the summit area. **d** Precipitation. *Vertical green lines* indicate eruptions; *red line* indicates a documented intrusion. *Vertical bars* indicate the periods of stable velocities used for averaging. *Horizontal lines* show the intervals where velocity changes are mapped

together with the upward component of surface deformation, summit seismicity, and precipitation rate (Huffman et al. 2001).

Common dynamics in the data shown in Fig. 3.8 is easily identified by means of the seismicity. Seismic crises exceeding more than 100 events per day are always reflected by abrupt deformation and velocity changes. During seismically quiet periods deformations show slow subsidence accompanied by a mostly steady velocity increase with an exception in the third quarter of 2010. A relation with precipitation cannot be established.

To map the spatial variability of the velocity changes we assume spatial continuity and interpolate linearly between estimates at the station locations. Here we focus on

two time intervals, I2 and R1 (Fig. 3.8) for which the distributions of velocity changes are shown in Fig. 3.9a and b, respectively.

Figure 3.9 shows maps of the velocity changes for two periods with clearly different types of processes. The first example (Fig. 3.9a) shows the time interval that includes the dyke intrusion on September 23, 2010 (I2 in Fig. 3.8). The intrusion was accompanied by a seismic crisis and caused surface deformation detected by the GPS network. It was also observed as a characteristic low frequency tilt signal at a neighboring seismic broad band station (Roult et al. 2012). Seismic velocities decreased during the intrusion by up to 0.4 %. While the outer part of the volcano remains at almost constant velocity the decrease concentrates around the summit area. Surface deformation during this time interval shows expansion and uplift around the summit.

The second example (Fig. 3.9b) shows the velocity changes that occurred between February and July, 2010 (R1 in Fig. 3.8). This is a period of quiescence that followed on intensive activity to the end of 2009 in which three eruptions occurred in two months. During this period there was no seismic activity at the summit and surface deformation indicates a steady but subtle deflation. Similarly, the seismic velocities show a constant steady increase. Geographically this increase is again focused around the summit area. Changes associated with eruptions are spatially heterogeneous but involve large scale velocity increase in the northern part of the volcano.

The two examples shown above are characteristic for the type of the dominant process. In our data set there are different episodes that are most likely associated with magmatic intrusions. These are the periods I3 preceding an eruption in December 2010 and the periods I4 and I5 that coincide with a seismic crisis in February 2011 (Fig. 3.8). All of them show a velocity decrease with a similar spatial distribution but variable amplitude to period I2 depicted in Fig. 3.9a. Also the remaining periods of quiescence indicated as R2-4 in Fig. 3.8 show the same pattern as period R1—a velocity increase concentrated around the summit.

Based on these characteristic changes of velocities our observations help to assess the state of activity of the volcano. The change in the velocity trend in July 2010 can for example be interpreted as a preparatory signal of the dyke intrusion in September. This occurred prior to any clear signal in the deformation time series. Also the interval between the eruptions in October and December can clearly be identified as affected by inflation rather than quiescence on the basis of the velocity changes indicating an increasing probability for an eruption that eventually occurred in December.

## 3.5 Summary

In the previous sections we described the two approaches followed in the MIIC-project to obtain a dynamic tomographic record of the subsurface that not only images the seismic velocity structure but also monitors its changes.

In Sect. 3.3 we described our newly developed technique to investigate the velocity distribution on an engineering scale from ambient seismic noise records using frequencies higher than a few Hz. The algorithm is very efficient as it performs a

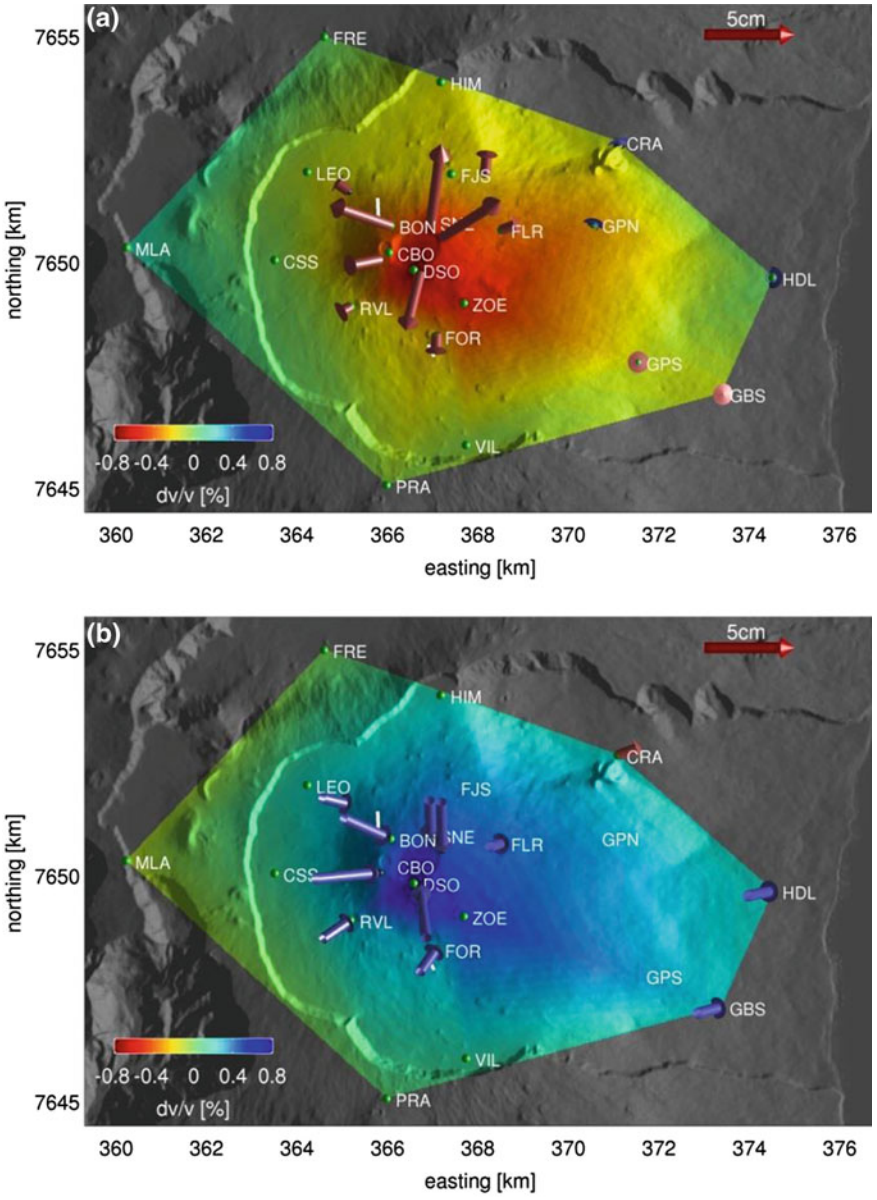


**Fig. 3.9** Distribution of velocity changes for two time intervals. *Green dots* represent seismic stations. *Arrows* denote surface deformation. *Red* (*blue*) *arrows* indicate uplift (subsidence) and point away (towards) the station. **a** Changes associated with the dyke intrusion in September 2010 (I2 in Fig. 3.8). **b** Gradual changes during a quiet period in 2010 (R1 in Fig. 3.8)

3D inversion directly on dispersion curves without a detour via velocity maps. We obtained high quality 3D images of subsurface structures along an active fault and on a landslide in central Asia. These applications demonstrate the possibility to use interferometric concepts for imaging on a spatial scale of several hundred meters.

As the required recording durations in this frequency range are of the order of several hours we are able to monitor velocity changes on a time scale below one day with high spatial resolution just by repeated tomographic inversions. This reaches the target of a dynamic tomography from the imaging side.

The complementary approach starting from noise based monitoring of scattered wave fields is described in Sect. 3.4. The application to the $CO_2$ storage test site illustrates the high precision that can be achieved by interferometry and allows to detect relative variations of seismic velocities of about 0.1 %. At Piton de la Fournaise volcano we show how information about the spatial distribution of the velocity changes can be obtained also from scattered wave fields. The resulting maps illustrate how the volcanic processes influence the seismic velocities. This way we obtain information about the dynamics of the volcano that is complementary to more conventional measurements such as seismicity and surface deformation. It demonstrates the success of augmenting the noise based monitoring with spatial resolution to obtain a dynamic tomography.

**Acknowledgments** The project MIIC is part of the R&D-Programme GEOTECHNOLOGIEN. It is funded by the German Ministry of Education and Research (BMBF), Grants/ Förderkennzeichen of sub-projects 03G0736A, 03G0736B, 03G0736C, 03G0736D, 03G0757A.

Data from Piton de la Fournaise was kindly provided by the UnderVolc project and the Observatoire volcanologique du Piton de la Fournaise.

## References

Aki K (1957) Space and time spectra of stationary stochastic waves, with a special reference to microtremors. Bull Earthq Res Inst Tokyo Univ 24:415–457

Bensen GD, Ritzwoller MH, Barmin MP, Levshin AL, Lin F, Moschetti MP, Shapiro NM, Yang Y (2007) Processing seismic ambient noise data to obtain reliable broad-band surface wave dispersion measurements. Geophys J Int 169:1239–1260

Bonnefoy-Claudet S, Cotton F, Bard PY (2006) The nature of noise wavefield and its applications for site effects studies: a literature review. Earth-Sci Rev 79:205–227

Brenguier F, Shapiro NM, Campillo M, Nercessian A, Ferrazzini V (2007) 3D surface wave tomography of the Piton de la Fournaise volcano using seismic noise correlations. Geophys Res Lett 34:L02305. doi:10.1029/2006GL028586

Brenguier F, Shapiro NM, Campillo M, Ferrazzini V, Duputel Z, Coutant O, Nercessian A (2008) Towards forecasting volcanic eruptions using seismic noise. Nat Geosci 1:126–130

Brenguier F, Kowalski P, Staudacher T, Ferrazzini V, Lauret F, Boissier P, Di Muro A (2012) First results from the underVolc high resolution seismic and GPS network deployed on Piton de la Fournaise volcano. Seismol Res Lett 83:97–102

Campillo M, Paul A (2003) Long-range correlations in the diffuse seismic coda. Science 299:547–549

Campillo M (2006) Phase and correlation in 'random' seismic fields and the reconstruction of the green function. Pure Appl Geophys 163:475–502

Curtis A, Gerstoft P, Sato H, Snieder R, Wapenaar K (2006) Seismic interferometry—turning noise into signal. Lead Edge 25:1082–1092

Curtis A, Halliday D (2010) Source-receiver wave field interferometry. Phys Rev E 81:1–10

Chávez-García FJ, Luzón F (2005) On the correlation of seismic microtremors. J Geophys Res 110:B11313. doi:10.1029/2005JB003671

Derode A, Larose E, Tanter M, de Rosny J, Tourin A, Campillo M, Fink M (2003) Recovering the Green's function from field-field correlations in an open scattering medium (L). J Acoust Soc Am 113:2973–2976

Fleming K, Picozzi M, Milkereit C, Kuhnlenz F, Lichtblau B, Fischer J, Zulfikar C, Özel O (2009) SAFER and EDIM working groups: the self-organizing seismic early warning information network (SOSEWIN). Seismol Res Lett 80(5):755–771

Forbriger T (2003) Inversion of shallow seismic wavefields. I. Wavefield transformation. Geophys J Int 153:719–734

Foti S, Comina C, Boiero D, Socco LV (2009) Non uniqueness in surface wave inversion and consequences on seismic site response analyses. Soil Dyn Earthq Eng 29:982–993

Halliday D, Curtis A (2008) Seismic interferometry, surface waves and source distribution. Geophys J Int 175:1067–1087

Huffman GJ, Adler RF, Morrissey M, Bolvin DT, Curtis S, Joyce R, McGavock B, Susskind J (2001) Global precipitation at one-degree daily resolution from multi-satellite observations. J Hydrometeor 2:36–50

Ivanova A, Kashubin A, Juhojuntti N, Kummerow J, Henninges J, Juhlin C, Lüth S, Ivandic M (2012) Monitoring and volumetric estimation of injected CO2 using 4D seismic, petrophysical data, core measurements and well logging: a case study at Ketzin, Germany. Geophys Prospect 60(5):957–973

Korjenkov AM, Kolchenko VA, Rott PG, Abdieva SV (2012) Strong mediaeval earthquakes in the Chuy basin, Kyrgyzstan. Geotectonics 46:303–314

Lobkis OI, Weaver RL (2001) On the emergence of the Green's function in the correlations of a diffuse field. J Acous Soc Am 110:3011–3017

Megies T, Beyreuther M, Barsch R, Krischer L, Wassermann J (2011) ObsPy-What can it do for data centers and observatories? Ann Geophys 54:47–58

Obermann A, Planes T, Larose E, Sens-Schönfelder C, Campillo M (2013) Depth sensitivity of seismic coda waves to velocity perturbations in an elastic heterogeneous medium. Geophys J Int 194(1):372–382

Parolai S, Orunbayev S, Bindi D, Strollo A, Usupayev S, Picozzi M, Di Giacomo D, Augliera P, D'Alema E, Milkereit C, Moldobekov B, Zschau J (2010) Site effect assessment in Bishkek (Kyrgyzstan) using earthquake and noise recording data. Bull Seismol Soc Am 100(6):3068–3082

Picozzi M, Parolai S, Bindi D, Strollo A (2009) Characterization of shallow geology by high-frequency seismic noise tomography. Geophys J Int 176:164–174

Pilz M, Parolai S, Picozzi M, Bindi D (2012) Three-dimensional shear wave velocity imaging by ambient seismic noise tomography. Geophys J Int 189:501–512

Pilz M, Parolai S, Bindi D (2013) 3D passive imaging of complex seismic fault systems: evidence of surface traces of the Issyk-Ata fault (Kyrgyzstan). Geophys J Int 194:1955–1965. doi:10.1093/gji/ggt214

Poupinet G, Ellsworth W, Frechet J (1984) Monitoring velocity variations in the crust using earthquake doublets: an application to the calaveras fault, California. J Geophys Res 89(4):5719–5731

Rickett J, Claerbout J (1999) Acoustic daylight imaging via spectral factorization: Helioseismology and reservoir monitoring. Lead Edge 18:957–960

Roult G, Peltier A, Taisne B, Staudacher T, Ferrazzini V, Di Muro A (2012) A new comprehensive classification of the Piton de la Fournaise activity spanning the 1985–2010 period. Search and analysis of short-term precursors from a broad-band seismological station. J Volcanol Geoth Res 241–242:78–104

Sens-Schönfelder C, Wegler U (2006) Passive image interferometry and seasonal variations of seismic velocities at Merapi Volcano, Indonesia. Geophys Res Lett 33(21):1–5

Sens-Schönfelder C, Wegler U (2011) Passive image interferometry for monitoring crustal changes with ambient seismic noise. C R Geosci 343:639–651

Snieder R, Grêt A, Douma H, Scales J (2002) Coda wave interferometry for estimating nonlinear behavior in seismic velocity. Science 295(5563):2253–5

Snieder R (2004) Extracting the Green's function from the correlation of coda waves: a derivation based on stationary phase. Phys Rev E 69:046610-1–046610-8

Weaver RL, Lobkis OI (2001) Ultrasonics without a source: thermal fluctuation correlations at MHz frequencies. Phys Rev Lett 87:134301-1–134301-4

Weaver RL, Lobkis OI (2004) Diffuse fields in open systems and the emergence of the greens function. J Acoust Soc Am 116:2731–2734